ACS OMEGA

http://pubs.acs.org/journal/acsodf

Article

Time−Frequency Characteristics and Evolution Law of Acoustic Emission Signals during the Deformation and Failure of Deformed Coal

Zhengshuai Liu, Longyong Shu,* Nannan Zhu, Zhonggang Huo, and Zhongxue Sun

Cite This: *ACS Omega* 2023, 8, 15799−15809

Read Online

ACCESS | Metrics & More | Article Recommendations

ABSTRACT: The research on the time−frequency characteristics and evolution law of acoustic emission (AE) signals during deformed coal failure is more conducive to understand the damage mechanism of coal. In this study, the experiments of AE monitoring during the intact and deformed coal failure were first conducted under loading axial stress and unloading confining stress conditions. Based on the evolution characteristics of volume strain and AE event rate, the damage process of coal was divided into three stages: nonfracture development stage, stable development stage of fracture, and unstable development stage of fracture. The distribution and evolution of AE waveform time−frequency properties under different damage processes were then analyzed and discussed. Besides, the evolution of the average value of different time−frequency parameters per 200 s for the intact coal and per 25 s for the deformed coal was discussed. The results show that the amplitude of most AE events stabilizes in 40−50 dB during the intact and deformed coal failure. The average amplitude of the deformed coal has an approximate positive correlation with the loading stress. The percentage of AE events with longer duration and rise time increases suddenly before the peak stress for the intact coal and after the peak stress for the deformed coal, which corresponds to the abrupt increase property of the average duration and rise time. For the frequency properties, the peak frequency and frequency centroid of the intact coal are distributed within 50−125 and 75−150 kHz, with those of the deformed coal located within 20−120 and 80−130 kHz, respectively. The average peak frequency and frequency centroid of the intact coal show an upward trend except for the initial fracture closure stage, while the average peak frequency and average frequency centroid of the deformed coal present a downward trend before the peak stress and have a smaller growth after the peak stress. According to the above-mentioned analysis, the sudden increase of the average duration and rise time, the lower average peak frequency, and the lower frequency centroid can be regarded as the precursor for the instability and failure of deformed coal. This research can provide a new idea and theoretical guidance for the early warning of outbursts.

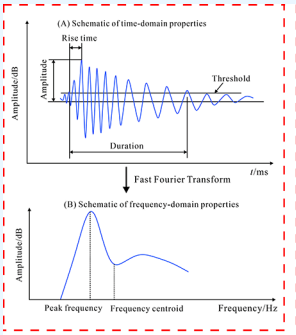

Schematic of AE time-frequency characteristics

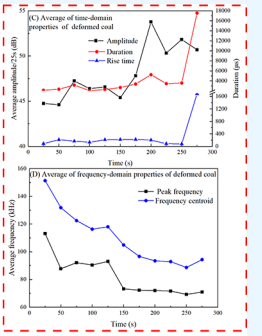

Evolution law of the average time-frequency parameters during the deformed coal failure

1. INTRODUCTION

Coal and gas outburst (hereafter outbursts) as one of the most serious disasters in coal mines threatens the safety of workers and the energy supply.[1,2] Previous studies on the outburst mechanism revealed that the stress, gas pressure, and physical and mechanical properties of coal in an abnormal geological zone determine the occurrence of outbursts.[3−5] The stress state and gas pressure in the front of the working face are influenced by the mining activities.[6,7] The acoustic emission (AE) event number/rate and gas emission that can reflect the stress state and gas pressure in the front of the working face in real time were used as precursors to warn about outbursts.[8,9] However, the accuracy of the outburst warning is limited using the AE event number/rate due to lots of interference signals existing in the field.[10] More precursory information from the AE waveform characteristics should be explored, which is meaningful for characterizing the early warning of outbursts.

The AE signals that are related to the fracture development have been widely utilized to study the failure mechanism of coal and rock under different stress loading conditions.[11−14] The AE statistical characteristics commonly used include the event rate, energy rate, ringing count, Ib value, and fractal dimension characteristics.[15−19] Du et al.[20] investigated the AE cumulative event counts and energy characteristics during deformation and failure of gas-bearing coal−rock combined bodies. Wang et al.[21] focused on the variation characteristics of AE energy during coal failure and confirmed the predicting key point of coal failure

Received: March 17, 2023
Accepted: April 7, 2023
Published: April 17, 2023

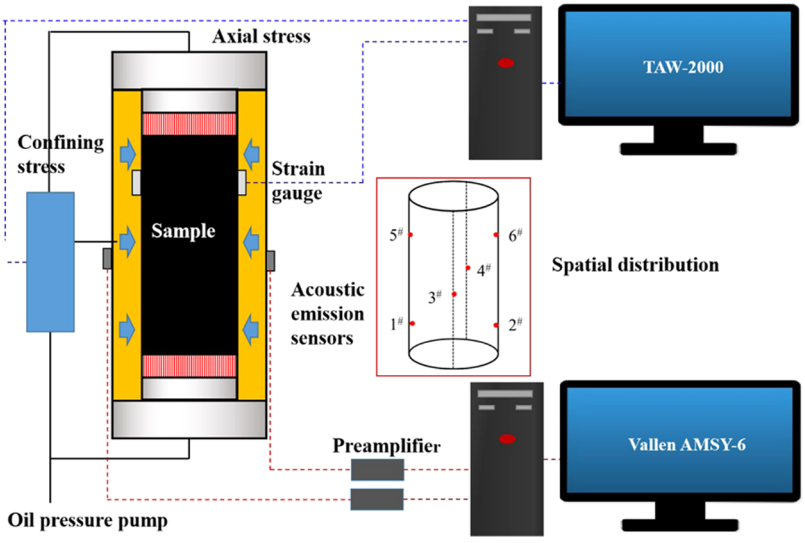

Figure 1. Diagram of the acoustic emission test during coal failure.

about two parameters related with the AE energy. Sun et al.[22] combined the fractal properties of AE event counts and stress with the Grassberger−Procaccia algorithms to evaluate the damage degree of coal and rock under multilevel loading. Huang et al.[23] analyzed the evolution of AE energy, Ib value, and fractal dimension characteristics in the sandstone failure process and found that there is a sharp increase of AE energy, lower Ib value, and lower shape dimension before the peak loading stress. The above-mentioned studies showed that the AE statistical characteristics can well indicate the stress state and fracture development during coal and rock failure.

Comparing the precursory information of AE statistical characteristics, the AE waveform properties may be more suitable for evaluating the failure of coal and rock and warning of outbursts.[24−27] The essential reason is that the AE statistical characteristics are seriously influenced by the accurate identification of coal failure due to lots of interference signals in the field.[8,28] The waveform characteristics widely used include amplitude, duration, rise time, dominant frequency, and frequency centroid.[28−30] Shen et al.[31] studied the amplitude and dominant frequency properties of AE during the coal fracturing process and discussed the influence of water pressure on the amplitude and dominant frequency variation. Zhao et al.[32] established the relationship between the AE frequency centroid and crack levels of sandstone failure and proposed the average frequency centroid variation as a precursor for rock critical failure. Ding et al.[24] and Wang et al.[33] used the Mel frequency cepstrum coefficient method to extract the AE waveform properties (MFCC), which were regarded as an indicator to evaluate the stress state of coal and rock. According to the above-mentioned studies, the AE waveform characteristic variation law during the rock failure and the AE statistical characteristics in the coal and rock failure process have made great progress, but there are few studies investigating the evolution law of AE waveform characteristics during coal deformation and failure, which is more important to warn about the outbursts. Considering that the existence of deformed coal is the necessary factor triggering the outbursts,[34−36] this paper focuses on the time−frequency characteristics and evolution law of the AE signal during the deformation and failure of deformed coal.

In this work, the experiments of AE monitoring during the intact and deformed coal failure were first conducted under loading axial stress and unloading confining stress conditions. The damage process was divided by the evolution characteristics of volume strain and AE event rate. The distribution and evolution of AE waveform time−frequency properties under different damage processes were then analyzed and discussed. The precursors of AE waveform characteristics for outburst warning were finally proposed. This research can provide a new idea and theoretical guidance to the early warning of outbursts.

2. EXPERIMENTAL SECTION

2.1. Samples. The coal samples including intact coal blocks and deformed coal fines were collected from the 3# coal seam of the Xinyuan coal mine, which was identified as a high-outburst seam. The intact coal blocks were directly cut into standard specimens with the dimensions of 50 mm diameter and 100 mm height. Due to the fragility properties of deformed coal, briquette coals were often used to investigate the coal failure mechanism of deformed coals due to their similar properties.[37,38] Briquette coals with a diameter of 50 mm and a height of 100 mm were prepared, and the detailed process can be found in our previous research.[39]

2.2. Experimental Setup. The experiments of AE monitoring during coal failure were conducted using a TAW-2000 rock triaxial test system and Vallen AMSY-6 AE monitoring system (shown in Figure 1).

The triaxial test system mainly consists of the axial and confining loading systems, strain gauges, and data acquisition equipment, which can provide different stress paths and monitor the stress−strain data in real time. The AE monitoring system is mainly composed of the sensors, preamplifier, data acquisition equipment, and analyzing software, which can obtain, display, storage, and deal with the AE signals. Six sensors with a frequency band from 15 to 500 kHz were arranged in the three-dimensional space to acquire the AE signals (Figure 1). The sampling rate, threshold, and amplification of the preamplifier were set as 1 MHz, 40 dB, and 34 dB, respectively. One event was defined when four or more sensors were triggered at the same time during the test.

2.3. Test Scheme. The triaxial stress evolution for the coal body in the front of the working face has an important role in the

https://doi.org/10.1021/acsomega.3c01815
ACS Omega 2023, 8, 15799−15809

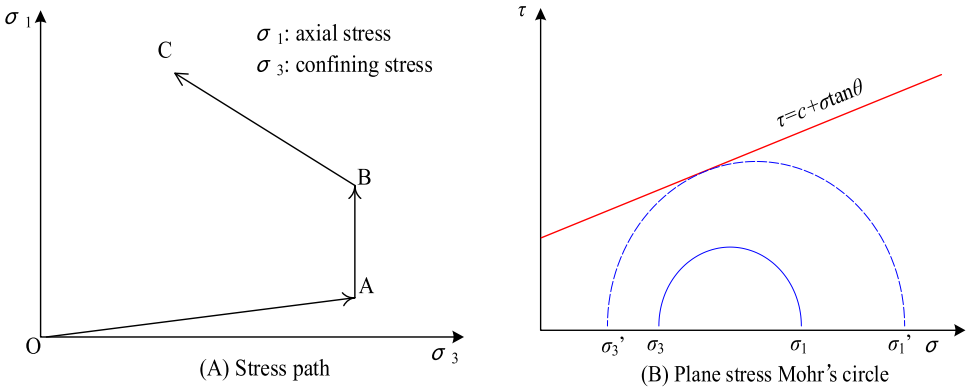

Figure 2. Schematic of stress paths and Mohr's stress circle.

coal deformation and failure. Previous studies showed that the vertical stress increases and the horizonal stress decreases during the excavation.[40] Therefore, the stress mode for loading axial stress and unloading confining stress was applied in this study. The evolution of stress paths and Mohr's circle is displayed in Figure 2. An axial stress of 300 N was first loaded on the specimen to ensure a close contact between the press indenter and the specimen. A loading rate of 5 N/s was then applied in the horizonal direction until the confining stress reaches the target value (OA in Figure 2). Under the constant confining stress, a loading rate of 20 N/s was imposed in the axial direction until the axial stress reaches 60% of the peak stress. After that, the axial stress increased continuously while unloading the confining stress at a rate of 5 N/s for intact coals and 40 N/s for briquette coals until the specimen's failure (BC in Figure 2). The acquisition of AE signals and stress−strain values is synchronized with the axial stress loading during the test (AC in Figure 2). In this study, the confining stress was set as 2, 4, 6, and 8 MPa for four groups of intact and deformed specimens (Table 1). Three parallel specimens were characterized under each confining stress condition. Besides, the above-mentioned loading and unloading rates were determined by carrying out pre-experiments.

Table 1. Test Scheme Parameters

coal structure	sample number	confining stress	coal structure	sample number	confining stress
intact coal	Y-2-1	2	deformed coal	X-2-1	2
	Y-2-2	4		X-2-2	4
	Y-2-3	6		X-2-3	6
	Y-2-4	8		X-2-4	8

3. RESULTS

3.1. Characteristics of the Strain and AE Event Rate during Coal Failure. The results of the intact coal specimen (Y-2-2) and deformed coal specimen (X-2-1) are used to investigate the time−frequency characteristics and evolution law during coal failure considering the space constraints. The coal damage is accompanied with the fracture closure, development, and expansion, which can be reflected by the stress−strain curve and evolution of AE parameters.[20,39] Based on the evolution characteristics of volume strain and AE event rate (AE event number per second) during coal failure (Figure 3), the whole process of coal damage can be divided into three stages: nonfracture development stage (0−874 s for the intact coal, 0−120 s for the deformed coal), stable development stage of fracture (875−1450 s for the intact coal, 121−250 s for the deformed coal), and unstable development stage of fracture (1451−1600 s for the intact coal, 251−276 s for the deformed coal).

In the nonfracture development stage, the volume strain is above 0, which indicates that the initial pore and fracture were closed with the increase of axial stress and decrease of confining stress. The event rate of intact coal is no more than 8, while the event rate of deformed coal is no more than 4, which indicates that there are a few AE events. Compared with the intact coal,

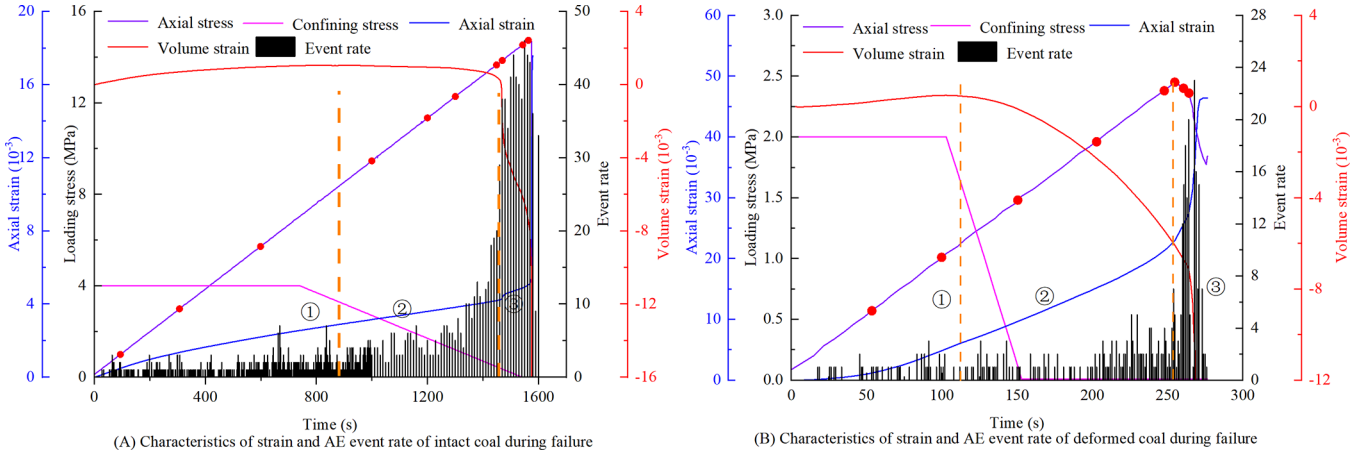

Figure 3. Characteristics of strain and AE event rate of intact and deformed coals during failure.

https://doi.org/10.1021/acsomega.3c01815
ACS Omega 2023, 8, 15799−15809

the AE events of the deformed coal are fewer, which is because the initial fracture in the deformed coal developed worse than that in the intact coal.[41]

In the stable development stage of fracture, the volume strain of the intact coal begins to decrease compared with that of the nonfracture development stage, which indicates that the fracture begins to form. Besides, the AE event rate increases obviously with the increase of the axial stress, which also indicates the development of fracture in the intact coal. While the volume strain of the deformed coal is lower, 0, which indicates the generation of fracture, the AE event rate of the deformed coal is still no more than 8, which is related to the strength of tectonic coal. In the unstable development stage of fracture, the volume strain rate (volume strain per second) of the intact and deformed coal increases rapidly, while the AE event rate also increases obviously, which implies the failure of coal and dissipation of the accumulated elastic energy. The maximum event rate of the intact coal reaches 44 before the peak axial stress, while the maximum event rate of the deformed coal reaches 23 after the peak axial stress. Compared with the evolution of the AE event rate of the intact coal, the property of an abrupt increase of the AE event rate is more obvious in the tectonic coal, and lots of AE events occur after the peak axial stress.

3.2. Distribution of AE Signal Time Domain Characteristics. The waveform parameters energy and ring count were widely used to investigate the mechanism of coal failure. The waveform parameters amplitude, rise time, and duration (illustrated in Figure 4A) also contain lots of information reflecting the coal failure, which were used to distinguish the microseismic signals of coal fracture.[8]

Figure 5 shows the distribution of the amplitude, duration, and rise time during coal failure. In the nonfracture development stage, the amplitude of the AE waveform is mainly distributed in 40−75 and 40−55 dB for the intact coal and the deformed coal, respectively. The duration of the AE waveform is relatively short, mainly distributed within 7000 and 5000 μs for the intact and deformed coal, respectively. The rise time of the AE waveform is also relatively short, mainly distributed within 2000 μs for the intact and deformed coal. In the stable development stage of fracture and unstable development stage of fracture, the amplitude of the AE waveform stabilizes in 40−85 and 40−74 dB for the intact and deformed coal, respectively. The appearance of high amplitude indicates the occurrence of great cracks. The distribution range of duration tends to increase with the gradual increase of the axial stress and decrease of the confining stress. The duration of the intact coal is distributed within 30 000 and 50 000 μs in the stable development stage of fracture and unstable development stage of fracture, respectively. The duration of the deformed coal in the stable development stage of fracture is only distributed within 16 000 μs but increases to 100 000 μs abruptly after the peak stress. Different from the distribution of duration, the rise time of the intact and deformed coal is still distributed within 2000 μs in the stable development stage of fracture and increases to 20 000 and 100 000 μs suddenly in the unstable development stage of fracture. The maximum rise time of the intact coal occurs before the peak stress, while it is after the peak stress for the deformed coal. Compared with the distribution of amplitude, duration, and rise time of the intact coal, the property of an abrupt increase of the duration and rise time of the deformed coal is more obvious after the peak stress.

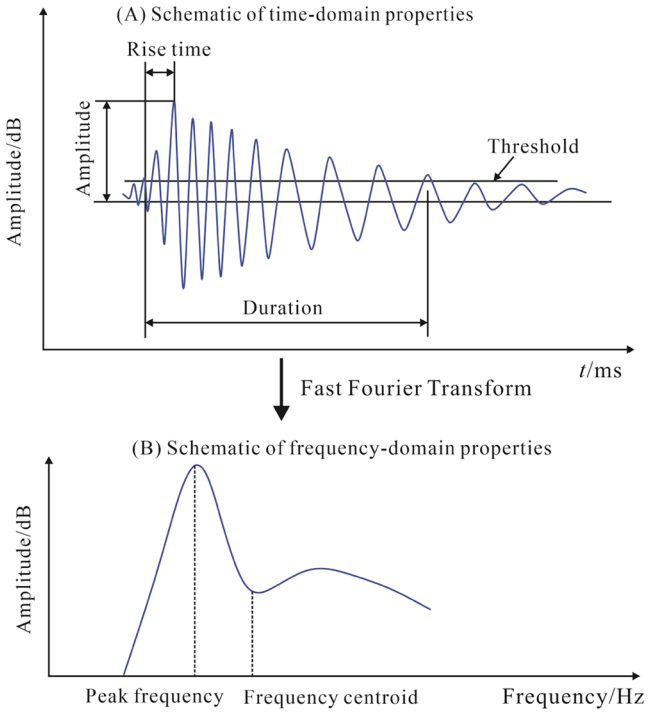

Figure 4. Illustration of AE waveform and frequency characteristics.

3.3. Distribution of AE Signal Frequency Domain Characteristics. The frequency information of the AE signal can be obtained by transforming the time−amplitude signal with the Fourier transform method.[42] The peak frequency (also called dominant frequency) and frequency centroid (the gravity of the frequency spectrum) illustrated in Figure 4B are two important parameters reflecting the frequency information of the AE signal, which were used to distinguish the different rocks.[43] In this study, the distributions of the peak frequency and frequency centroid during the intact and deformed coal failure are investigated and displayed in Figure 6.

During the whole process of coal failure, the peak frequency is mainly distributed within 50−125 kHz for the intact coal and 20−120 kHz for the deformed coal. There are also a few AE events whose peak frequency is located in 25−50 and 150−175 kHz for the intact coal and in 140−180 kHz for the deformed coal. Before the peak stress of the intact coal, the events of the peak frequency located in 25−50 and 150−175 kHz increase obviously, while the peak frequency of the deformed coal shifts toward lower frequencies with the increase of loading stress. Different from the peak frequency, the frequency centroid is mainly distributed within 75−150 kHz for the intact coal and 80−130 kHz for the deformed coal. However, the distribution of the frequency centroid of the intact coal is similar to the distribution of the peak frequency. Before the peak stress, the events of the frequency centroid lower than 75 kHz and higher than 150 kHz increase obviously for the intact coal, while the events of the frequency centroid lower than 80 kHz and higher than 130 kHz also increase after the peak stress of the deformed coal. The above-mentioned results prove that the difference of the peak frequency band and frequency centroid band exists in the intact and deformed coal.

4. DISCUSSION

4.1. Evolution Law of Time Domain Characteristics in Different Ranges. The distribution of the amplitude, duration, and rise time of the AE signal indicates that the time domain

https://doi.org/10.1021/acsomega.3c01815
ACS Omega 2023, 8, 15799−15809

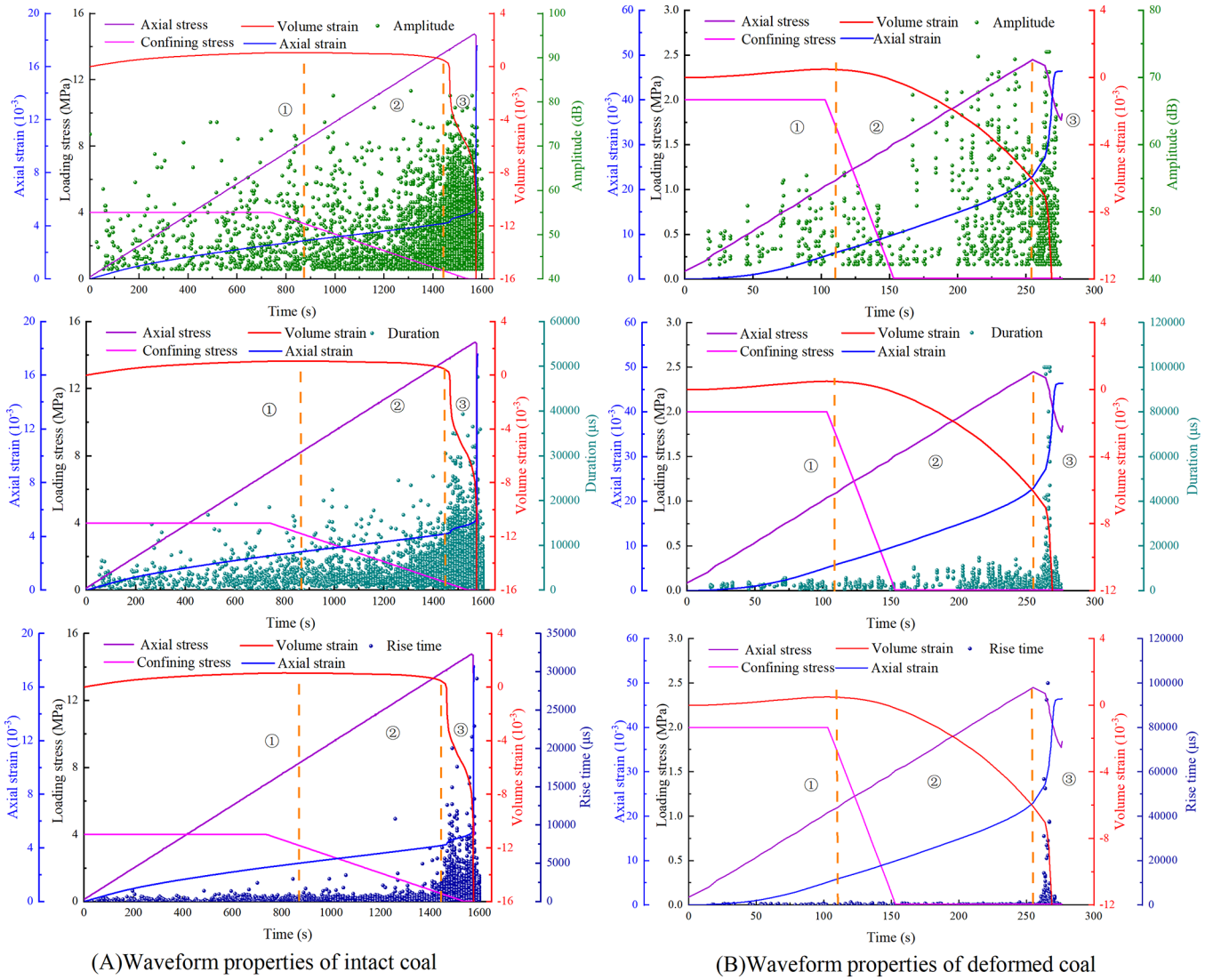

Figure 5. Distribution of waveform properties of intact and deformed coal during failure.

characteristics locate in different ranges during coal failure. To further illustrate the evolution law of time domain characteristics, the event number (per 200 s for the intact coal and per 25 s for the deformed coal) and its percentage of different time domain characteristics are counted and displayed in Figure 7 (intact coal) and Figure 8 (deformed coal).

From Figure 7A, it is observed that the event number of the amplitude in different ranges per 200 s increases with the increase of loading stress, especially for the amplitude in 40−60 dB before the peak stress, while the event number percentage (ENP) of the amplitude in different ranges has a small fluctuation. The ENP of the amplitude in 40−50 dB is the biggest, stabilizing at 75%. The amplitude over 60 dB only occupies 5−10%. From Figure 7B,C, it is observed that the event number of the duration and rise time in different ranges per 200 s also increase with the increase of loading stress, especially for the duration in 0−5000 μs and the rise time in 0−500 μs, while the ENP of the duration in 0−5000 μs and the rise time in 0−500 μs decline with the increase of the loading stress, almost from 92 and 93 to 67 and 68%. However, the event number and ENP for the duration over 5000 μs and the rise time over 500 μs gradually increase with the increase of loading stress and achieve the highest value before the peak stress. The increase of long duration and rise time indicates the occurrence of great cracks, which may be a precursor for outburst warning.

Similar to the change trends of the event number of different time domain properties in different ranges per 200 s for the intact coal, the event number of the amplitude, duration, and rise time in different ranges per 25 s for the deformed coal shows an upward trend overall with the increase of loading stress, especially for the amplitude in 40−50 dB, the duration in 0−5000 μs, and the rise time in 0−300 μs (Figure 8), while the ENP of the amplitude in 40−50 dB, duration in 0−5000 μs, and rise time in 0−300 μs shows a downward trend, from 100 to 62, 67, and 68%. The ENP of the duration over 15 000 μs and the rise time over 900 μs increases obviously after the peak stress, which is related with the release of great energy and indicates the coal failure.

4.2. Evolution Law of Frequency Domain Characteristics in Different Ranges. The event number (per 200 s for the intact coal and per 25 s for the deformed coal) and its percentage of peak frequency and frequency centroid in different ranges are also counted to further illustrate the evolution law of frequency domain characteristics. The statistical results are shown in Figure 9 (intact coal) and Figure 10 (deformed coal).

https://doi.org/10.1021/acsomega.3c01815
ACS Omega 2023, 8, 15799−15809

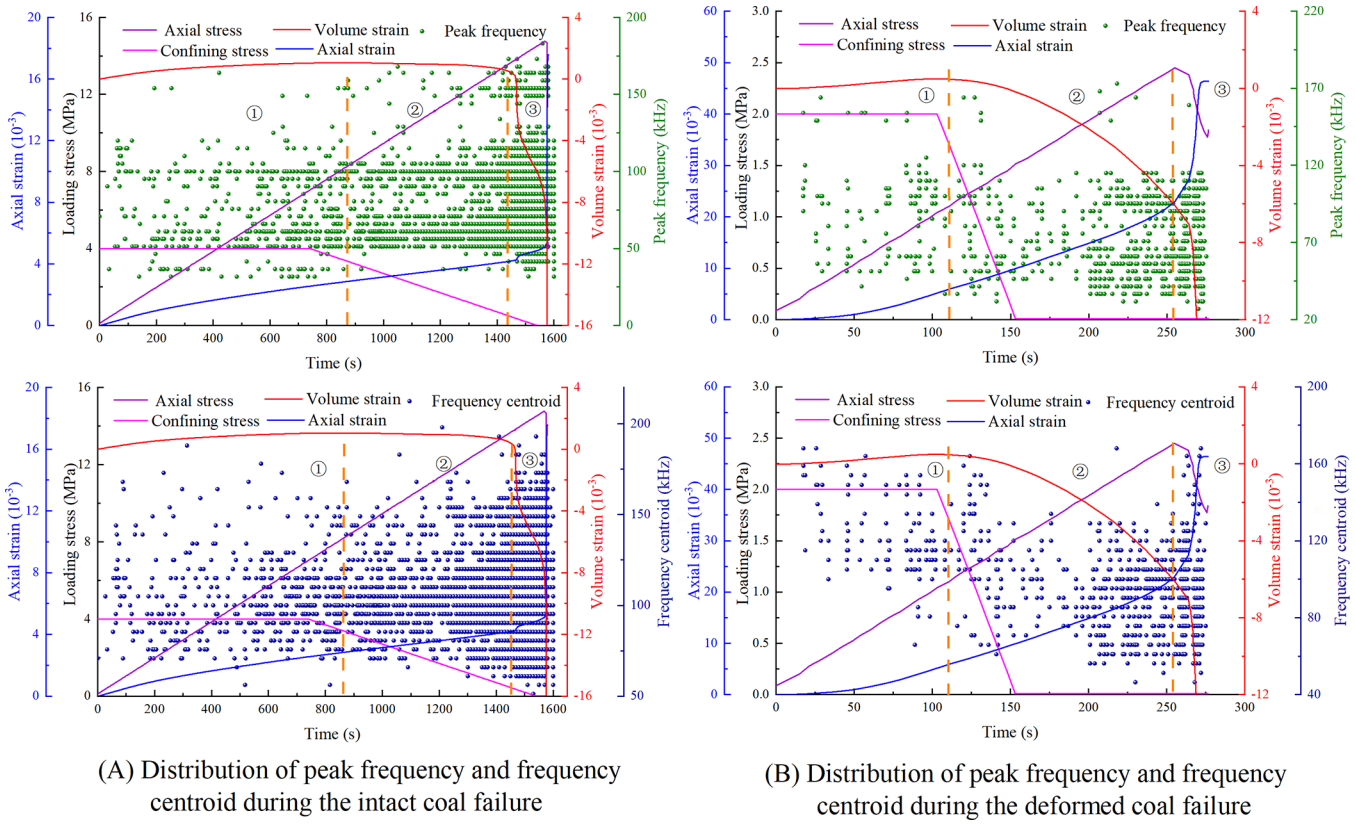

Figure 6. Distribution of frequency properties of intact and deformed coal during failure.

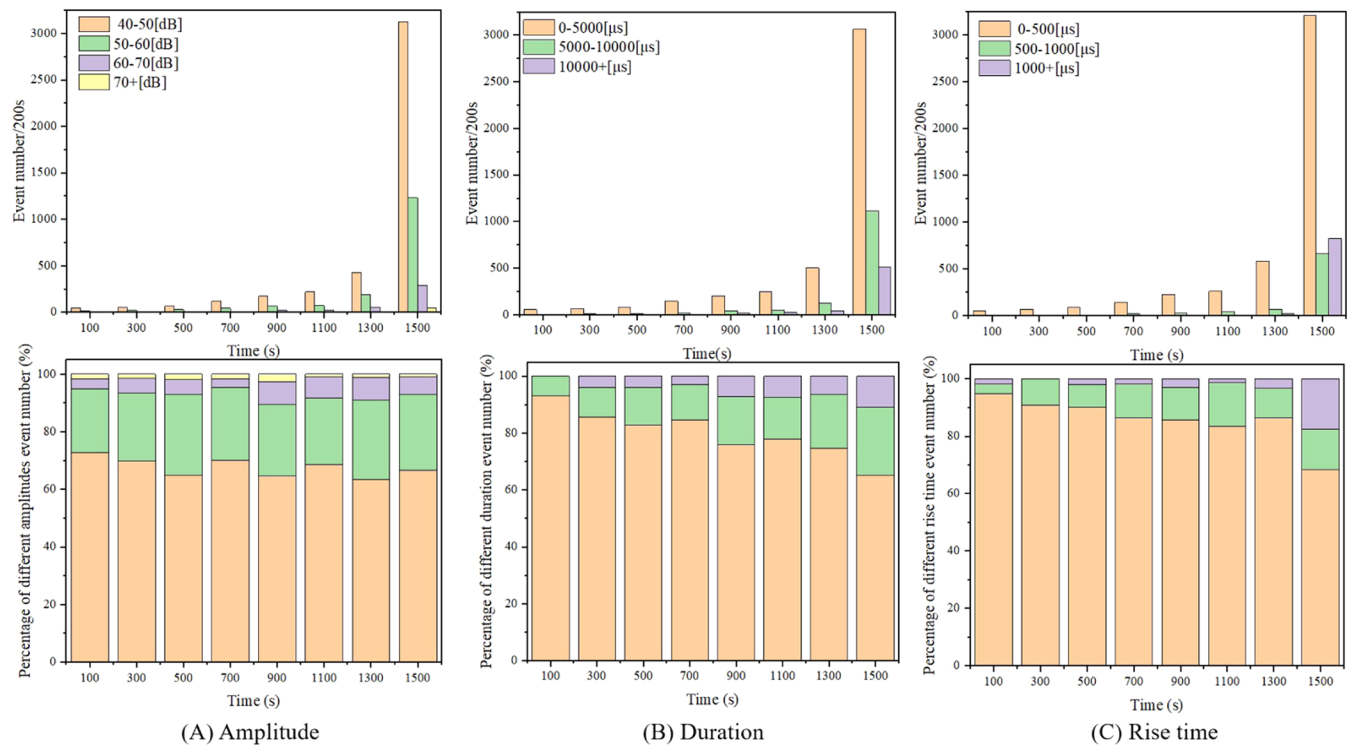

Figure 7. Evolution law of the amplitude, duration, and rise time in different ranges of the intact coal.

From Figure 9, it is observed that the event number of the peak frequency in 50−75 kHz and the frequency centroid in 100−125 kHz shows an obvious upward trend with the increase of the loading stress, while the abrupt increase of the event number for the peak frequency and frequency centroid in different ranges occurs before the peak stress. The ENP of the peak frequency and frequency centroid in different ranges has a stable fluctuation. The ENP of the peak frequency in 100−125

https://doi.org/10.1021/acsomega.3c01815
ACS Omega 2023, 8, 15799−15809

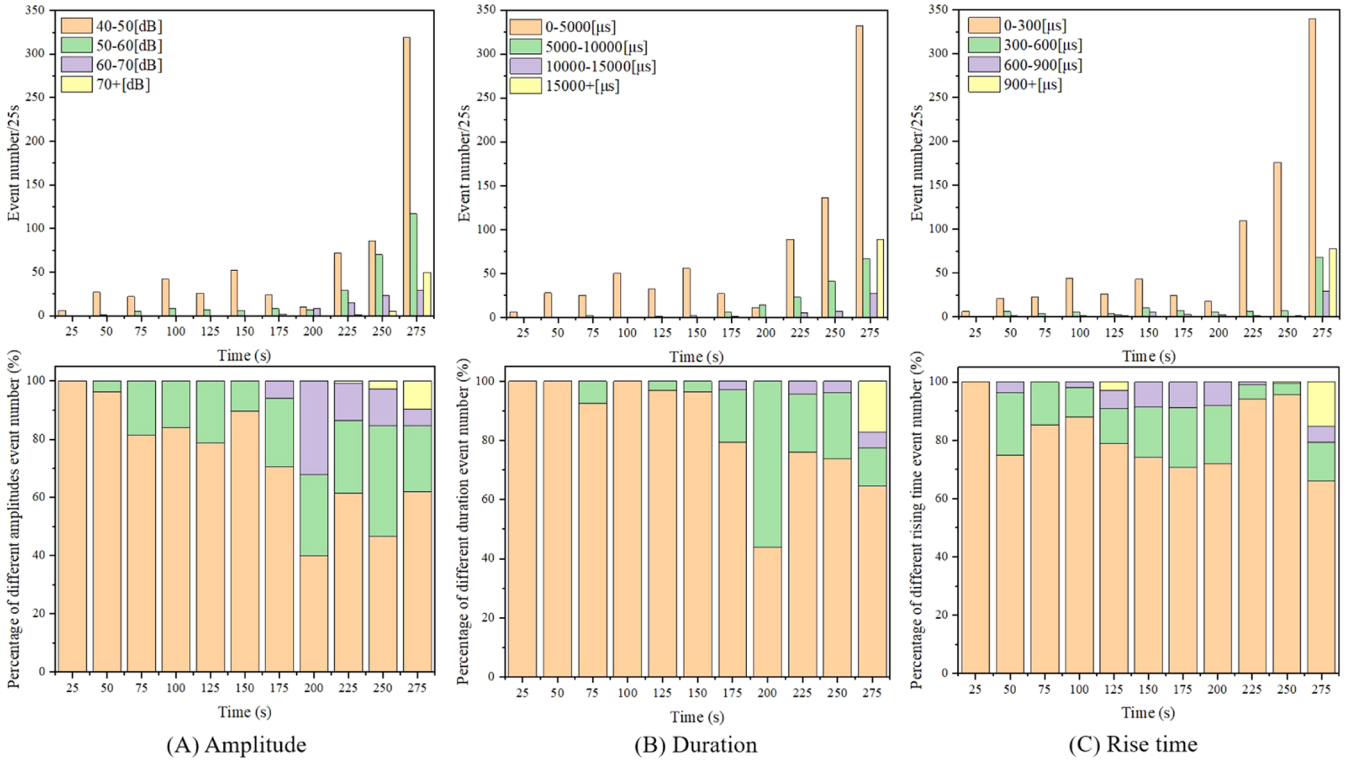

Figure 8. Evolution law of the amplitude, duration, and rise time in different ranges of the deformed coal.

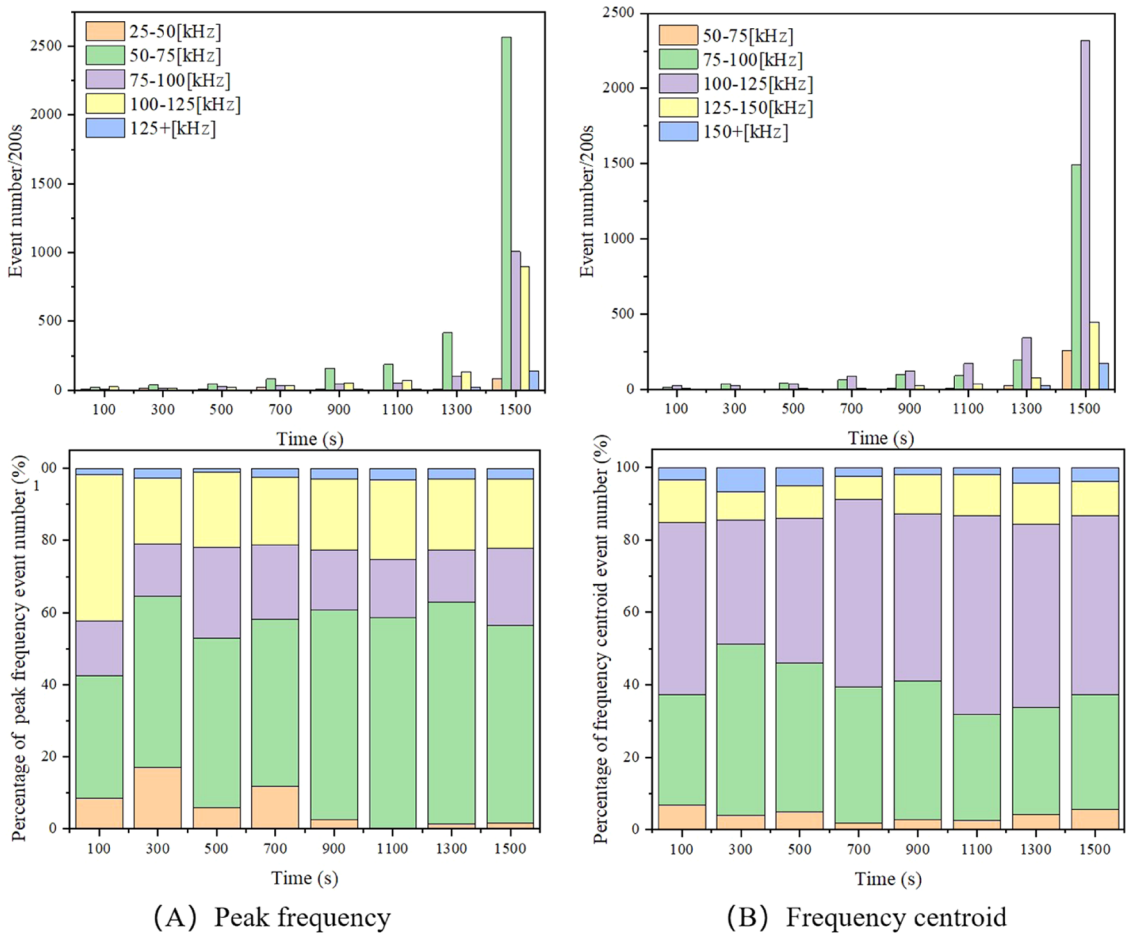

Figure 9. Evolution law of the peak frequency and frequency centroid in different ranges of the intact coal.

https://doi.org/10.1021/acsomega.3c01815
ACS Omega 2023, 8, 15799−15809

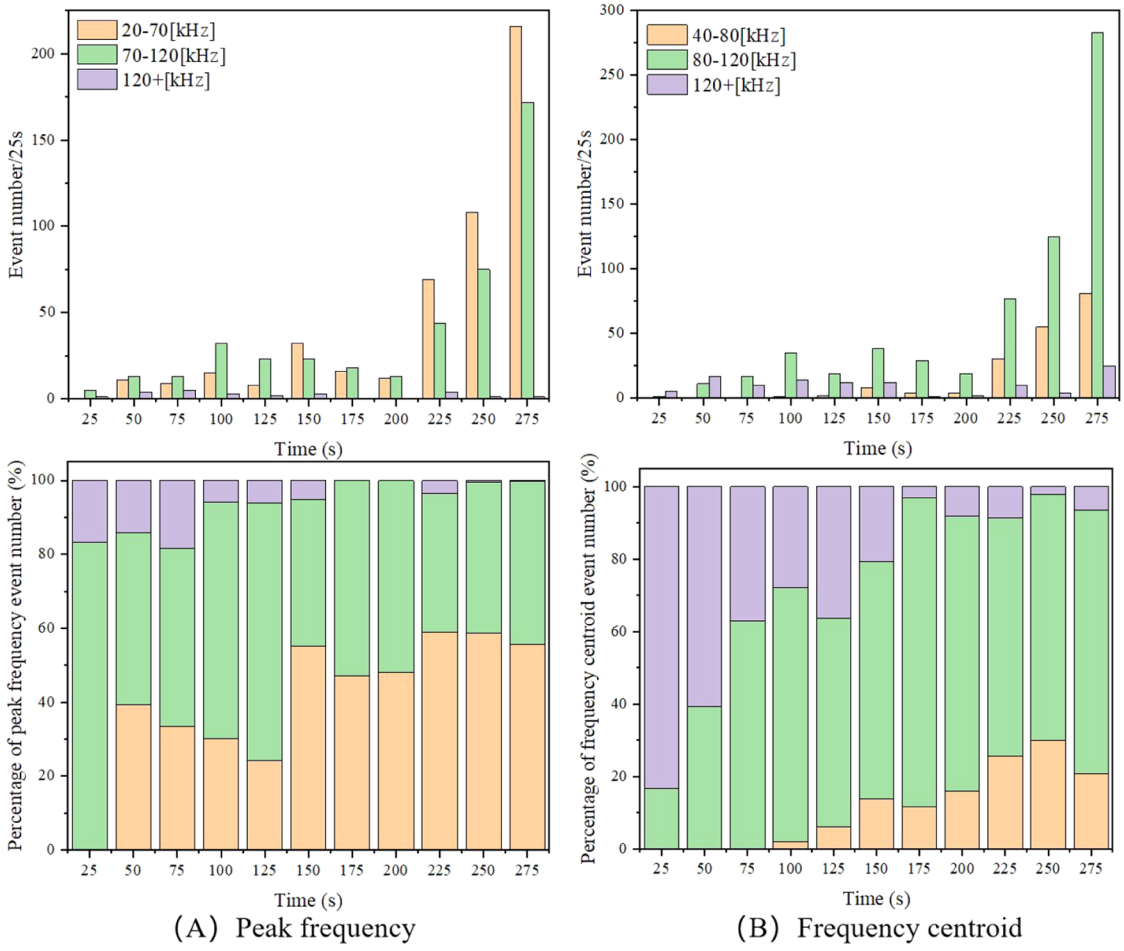

Figure 10. Evolution law of the peak frequency and frequency centroid in different ranges of the deformed coal.

kHz is the biggest in the initial stage, about 40%, and then stabilizes at about 18%, while the percentage of the peak frequency in 50−75 kHz shows an upward trend, ranging from 32 to 52%.

Compared with the evolution of frequency domain characteristics in different ranges of the intact coal, the event number of the peak frequency in 20−120 kHz and the frequency centroid in 80−120 kHz shows an obvious upward trend with the increase of the loading stress for the deformed coal (Figure 10). The fluctuation range of the ENP of the peak frequency and frequency centroid in different ranges is more obvious than that of the intact coal. The percentage of the peak frequency over 70 kHz shows a downward trend, while the percentage of the peak frequency in 20−70 kHz shows an upward trend. Different from the peak frequency, the percentage of the frequency centroid over 120 kHz displays a downward trend, while the percentage of the frequency centroid in 40−80 and 80−120 kHz displays an upward trend, especially for the frequency centroid in 40−80 kHz. According to the above-mentioned analysis, there are more AE events with a lower peak frequency (20−70 kHz) and lower frequency centroid (40−80 kHz) close to the coal failure, whose evolution law is similar with that of the previous study.[31]

4.3. Implication for Outburst Warning. The above-mentioned analysis indicates that there are different and same evolution characteristics of time−frequency parameters in different ranges of the AE signal for the intact and deformed coal. To further obtain the precursor information for outburst warning, the average value of different time−frequency parameters per 200 s for the intact coal and per 25 s for the deformed coal is calculated.

Figure 11 presents the evolution of average amplitude, duration, rise time, peak frequency, and frequency centroid of the intact and deformed coal. From Figure 11A,B, it is observed that the average amplitude is relatively low in the nonfracture development stage and increases and stabilizes with the increase of loading stress for the intact coal, while the average amplitude of the deformed coal first increases and then decreases with the increase of loading stress. The whole fluctuation range of the average amplitude is limited for the intact and deformed coal, which may not be a precursor for outburst warning. The average duration and average rise time increase with the increase of loading stress. There is an abrupt increase behavior for the intact coal before the peak stress, while the average duration and average rise time for the deformed coal are relatively stable before the peak stress and also have a sudden increase behavior after the peak stress, which can be regarded as a precursor for the great crack of the coal seam.

Comparing Figure 11C,D, it is observed that there are different evolution trends of the average peak frequency and frequency centroid between the intact coal and deformed coal, which may be used to distinguish the coal structures. The average peak frequency and frequency centroid of the intact coal in 0−200 s are relatively high, which indicate that the closure of the fracture presents high-frequency properties. From 400 to 1600 s, the average peak frequency and frequency centroid of the intact coal show an upward trend, while the average peak

https://doi.org/10.1021/acsomega.3c01815
ACS Omega 2023, 8, 15799−15809

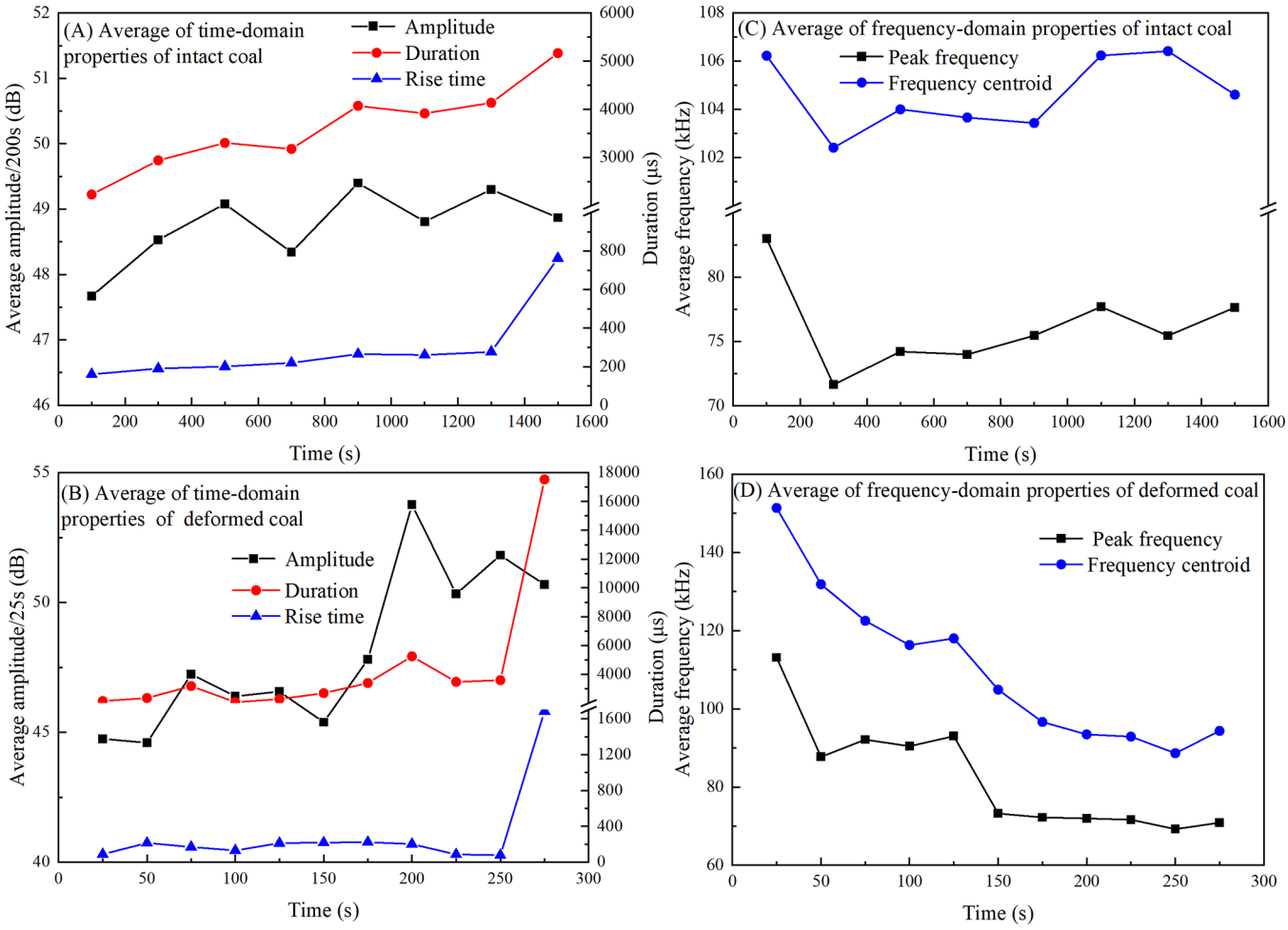

Figure 11. Evolution trend of the average time−frequency parameters during the intact and deformed coal failure.

frequency and average frequency centroid of the deformed coal present a downward trend before the peak stress and have a smaller growth after the peak stress. Because the outbursts mainly occurred in the geotectonic and soft coal development areas,[34,36] the lower average peak frequency and lower average frequency centroid may be regarded as the precursor for the instability and failure of deformed coal, which is conducive to guide the early warning of outbursts.

5. CONCLUSIONS

In this work, the experiments of AE monitoring during the intact and deformed coal failure under loading axial stress and unloading confining stress conditions were conducted to investigate the time−frequency characteristics and evolution law of the AE signal during coal failure. The main conclusions are drawn as follows:

(1) The coal damage process can be divided into three stages—nonfracture development stage, stable development stage of fracture, and unstable development stage of fracture—according to the evolution characteristics of volume strain and AE event rate during coal failure.

(2) The maximum AE event rate of the intact coal reaches 44 before the peak axial stress, while it reaches 23 after the peak axial stress for the deformed coal. The property of an abrupt increase of the AE event rate before failure is more obvious in the tectonic coal.

(3) The average amplitude of the deformed coal has an approximate positive correlation with the loading stress. The average duration and rise time have a sudden increase behavior after the peak stress for the deformed coal, which can be regarded as a precursor for the instability and failure of the deformed coal.

(4) The average peak frequency and average frequency centroid of the deformed coal present a downward trend before the peak stress and have a smaller growth after the peak stress. The lower average peak frequency and lower average frequency centroid may be regarded as the precursor for the instability and failure of deformed coal.

AUTHOR INFORMATION

Corresponding Author

Longyong Shu − *China Coal Research Institute, Beijing 100013, China*; Email: slyccri@163.com

Authors

Zhengshuai Liu − *Chinese Institute of Coal Science, Beijing 100013, China; China Coal Research Institute, Beijing 100013, China;* orcid.org/0009-0008-7630-0305

Nannan Zhu − *China Coal Research Institute, Beijing 100013, China*

Zhonggang Huo − *China Coal Research Institute, Beijing 100013, China*

https://doi.org/10.1021/acsomega.3c01815
ACS Omega 2023, 8, 15799−15809

Zhongxue Sun − *China Coal Research Institute, Beijing 100013, China*

Complete contact information is available at: https://pubs.acs.org/10.1021/acsomega.3c01815

Notes

The authors declare no competing financial interest.

■ ACKNOWLEDGMENTS

This research was funded by the Postdoctoral Research Foundation of China (Grant No. 2022M721450), the National Natural Science Fund of China (Grant Nos. 52174187, 51704164, 52130409), and the Technology Innovation Fund of China Coal Research Institute (Grant No. 2020CX-I-07).

■ REFERENCES

(1) Xue, S.; Tu, Q.; Hao, Y.; Yang, Y.; Zhao, Z.; Li, X. Occurrence and development criteria of coal and gas outbursts based on energy conversion. *Fuel* **2023**, *341*, No. 127781.

(2) Soleimani, F.; Si, G.; Roshan, H.; Zhang, Z. Numerical modelling of coal and gas outburst initiation using energy balance principles. *Fuel* **2023**, *334*, No. 126687.

(3) Shu, L.; Wang, K.; Liu, Z.; Zhao, W.; Zhu, N.; Lei, Y. A novel physical model of coal and gas outbursts mechanism: Insights into the process and initiation criterion of outbursts. *Fuel* **2022**, *323*, No. 124305.

(4) Zhou, B.; Xu, J.; Peng, S.; Yan, F.; Gao, Y.; Li, Q.; Cheng, L. Effects of geo-stress on the dynamic response of multi-physical field parameters during coal and gas outbursts under true triaxial stress. *Int. J. Rock Mech. Min. Sci.* **2021**, *142*, No. 104759.

(5) Li, W.; Ren, T.; Busch, A.; Den Hartog, S. A. M.; Cheng, Y.; Qiao, W.; Li, B. Architecture, stress state and permeability of a fault zone in Jiulishan coal mine, China: Implication for coal and gas outbursts. *Int. J. Coal Geol.* **2018**, *198*, 1−13.

(6) Shu, L.; Yuan, L.; Li, Q.; Xue, W.; Zhu, N.; Liu, Z. Response characteristics of gas pressure under simultaneous static and dynamic load: Implication for coal and gas outburst mechanism. *Int. J. Min. Sci. Technol.* **2023**, *33*, 155−171.

(7) Cao, A.; Jing, G.; Ding, Y.-l.; Liu, S. Mining-induced static and dynamic loading rate effect on rock damage and acoustic emission characteristic under uniaxial compression. *Saf. Sci.* **2019**, *116*, 86−96.

(8) Shu, L.; Liu, Z.; Wang, K.; Zhu, N.; Yang, J. Characteristics and classification of microseismic signals in heading face of coal mine: Implication for coal and gas outburst warning. *Rock Mech. Rock Eng.* **2022**, *55*, 6905−6919.

(9) Si, G.; Durucan, S.; Jamnikar, S.; Lazar, J.; Abraham, K.; Korre, A.; Shi, J.; Zavšek, S.; Mutke, G.; Lurka, A. Seismic monitoring and analysis of excessive gas emissions in heterogeneous coal seams. *Int. J. Coal Geol.* **2015**, *149*, 41−54.

(10) Yang, J.; Mu, Z.-L.; Yang, S.-Q. Experimental study of acoustic emission multi-parameter information characterizing rock crack development. *Eng. Fract. Mech.* **2020**, *232*, No. 107045.

(11) Du, X.; Xue, J.; Shi, Y.; Cao, C.; Shu, C.; Li, K.; Ma, Q.; Zhan, K.; Chen, Z.; Wang, S. Triaxial mechanical behaviour and energy conversion characteristics of deep coal bodies under confining pressure. *Energy* **2023**, *266*, No. 126443.

(12) Li, S.; Yang, D.; Huang, Z.; Gu, Q.; Zhao, K. Acoustic emission characteristics and failure mode analysis of rock failure under complex stress state. *Theor. Appl. Fract. Mech.* **2022**, *122*, No. 103666.

(13) Huang, J.; Hu, Q.; Qin, C.; Song, Z.; Wang, X. Pre-peak acoustic emission characteristics of tight sandstone failure under true triaxial stress. *J. Nat. Gas Sci. Eng.* **2022**, *102*, No. 104576.

(14) Jiang, C.; Duan, M.; Yin, G.; Wang, J. G.; Lu, T.; Xu, J.; Zhang, D.; Huang, G. Experimental study on seepage properties, AE characteristics and energy dissipation of coal under tiered cyclic loading. *Eng. Geol.* **2017**, *221*, 114−123.

(15) Zhang, L.; Ren, T.; Li, X.; Tan, L. Acoustic emission, damage and cracking evolution of intact coal under compressive loads: Experimental and discrete element modelling. *Eng. Fract. Mech.* **2021**, *252*, No. 107690.

(16) Liu, S.; Li, X.; Li, Z.; Chen, P.; Yang, X.; Liu, Y. Energy distribution and fractal characterization of acoustic emission (AE) during coal deformation and fracturing. *Measurement* **2019**, *136*, 122−131.

(17) Li, J.; Yue, J.; Yang, Y.; Zhan, X.; Zhao, L. Multi-resolution feature fusion model for coal rock burst hazard recognition based on acoustic emission data. *Measurement* **2017**, *100*, 329−336.

(18) Kong, X.; Wang, E.; Hu, S.; Shen, R.; Li, X.; Zhan, T. Fractal characteristics and acoustic emission of coal containing methane in triaxial compression failure. *J. Appl. Geophys.* **2016**, *124*, 139−147.

(19) Liu, J.; Li, Q.; Wang, X.; Wang, Z.; Lu, S.; Sa, Z.; Wang, H. Dynamic multifractal characteristics of acoustic emission about composite coal-rock samples with different strength rock. *Chaos, Solitons Fractals* **2022**, *164*, No. 112725.

(20) Du, F.; Wang, K.; Wang, G.; Jiang, Y.; Xin, C.; Zhang, X. Investigation of the acoustic emission characteristics during deformation and failure of gas-bearing coal-rock combined bodies. *J. Loss Prev. Process Ind.* **2018**, *55*, 253−266.

(21) Wang, C.; Hou, X.; Liao, Z.; Chen, Z.; Lu, Z. Experimental investigation of predicting coal failure using acoustic emission energy and load-unload response ratio theory. *J. Appl. Geophys.* **2019**, *161*, 76−83.

(22) Sun, H.; Liu, X. L.; Zhu, J. B. Correlational fractal characterisation of stress and acoustic emission during coal and rock failure under multilevel dynamic loading. *Int. J. Rock Mech. Min. Sci.* **2019**, *117*, 1−10.

(23) Huang, Z.; Gu, Q.; Wu, Y.; Wu, Y.; Li, S.; Zhao, K.; Zhang, R. Effects of confining pressure on acoustic emission and failure characteristics of sandstone. *Int. J. Min. Sci. Technol.* **2021**, *31*, 963−974.

(24) Ding, Z.; Li, X.; Huang, X.; Wang, M.; Tang, Q.; Jia, J. Feature extraction, recognition, and classification of acoustic emission waveform signal of coal rock sample under uniaxial compression. *Int. J. Rock Mech. Min. Sci.* **2022**, *160*, No. 105262.

(25) Li, B.; Wang, E.; Shang, Z.; Liu, X.; Li, Z.; Li, B.; Wang, H.; Niu, Y.; Song, Y. Optimize the early warning time of coal and gas outburst by multi-source information fusion method during the tunneling process. *Process Saf. Environ. Prot.* **2021**, *149*, 839−849.

(26) Li, N.; Huang, B.; Zhang, X.; Yuyang, T.; Li, B. Characteristics of microseismic waveforms induced by hydraulic fracturing in coal seam for coal rock dynamic disasters prevention. *Saf. Sci.* **2019**, *115*, 188−198.

(27) Kong, B.; Wang, E.; Li, Z.; Wang, X.; Niu, Y.; Kong, X. Acoustic emission signals frequency-amplitude characteristics of sandstone after thermal treated under uniaxial compression. *J. Appl. Geophys.* **2017**, *136*, 190−197.

(28) Li, B.; Wang, E.; Shang, Z.; Li, Z.; Li, B.; Liu, X.; Wang, H.; Niu, Y.; Wu, Q.; Song, Y. Deep learning approach to coal and gas outburst recognition employing modified AE and EMR signal from empirical mode decomposition and time-frequency analysis. *J. Nat. Gas Sci. Eng.* **2021**, *90*, No. 103942.

(29) Zhang, E.; Zhou, B.; Yang, L.; Li, C.; Li, P. Experimental study on the microseismic response characteristics of coal and gas outbursts. *Process Saf. Environ. Prot.* **2023**, *172*, 1058−1071.

(30) Qiu, L.; Song, D.; Li, Z.; Liu, B.; Liu, J. Research on AE and EMR response law of the driving face passing through the fault. *Saf. Sci.* **2019**, *117*, 184−193.

(31) Shen, R.; Qiu, L.; Zhao, E.; Han, X.; Li, H.; Hou, Z.; Zhang, X. Experimental study on frequency and amplitude characteristics of acoustic emission during the fracturing process of coal under the action of water. *Saf. Sci.* **2019**, *117*, 320−329.

(32) Zhao, K.; Yang, D.; Gong, C.; Zhuo, Y.; Wang, X.; Zhong, W. Evaluation of internal microcrack evolution in red sandstone based on time−frequency domain characteristics of acoustic emission signals. *Constr. Build. Mater.* **2020**, *260*, No. 120435.

(33) Wang, H. L.; Song, D. Z.; Li, Z. L.; He, X. Q.; Lan, S. R.; Guo, H. F. Acoustic emission characteristics of coal failure using automatic

speech recognition methodology analysis. *Int. J. Rock Mech. Min. Sci.* **2020**, *136*, No. 104472.
(34) Tu, Q.; Xue, S.; Cheng, Y.; Zhang, W.; Shi, G.; Zhang, G. Experimental study on the guiding effect of tectonic coal for coal and gas outburst. *Fuel* **2022**, *309*, No. 122087.
(35) Gao, D.; Sang, S.; Liu, S.; Wu, J.; Geng, J.; Tao, W.; Sun, T. Experimental study on the deformation behaviour, energy evolution law and failure mechanism of tectonic coal subjected to cyclic loads. *Int. J. Min. Sci. Technol.* **2022**, *32*, 1301−1313.
(36) Lu, S.; Wang, C.; Liu, Q.; Zhang, Y.; Liu, J.; Sa, Z.; Wang, L. Numerical assessment of the energy instability of gas outburst of deformed and normal coal combinations during mining. *Process Saf. Environ. Prot.* **2019**, *132*, 351−366.
(37) Liu, Q.; Zhang, K.; Zhou, H.; Cheng, Y.; Zhang, H.; Wang, L. Experimental investigation into the damage-induced permeability and deformation relationship of tectonically deformed coal from Huainan coalfield, China. *J. Nat. Gas Sci. Eng.* **2018**, *60*, 202−213.
(38) Skoczylas, N.; Dutka, B.; Sobczyk, J. Mechanical and gaseous properties of coal briquettes in terms of outburst risk. *Fuel* **2014**, *134*, 45−52.
(39) Shu, L.; Wang, K.; Zhang, L.; Sun, Z.; Hao, J.; Li, H. Investigation on acoustic emission behaviour evolution characteristics of outburst coal under uniaxial compression. *J. Min. Saf. Eng.* **2018**, *22*, 589−597.
(40) Xue, D.; Wang, J.; Zhao, Y.; Zhou, H. Quantitative determination of mining-induced discontinuous stress drop in coal. *Int. J. Rock Mech. Min. Sci.* **2018**, *111*, 1−11.
(41) Wang, Z.; Cheng, Y.; Wang, L.; Zhou, H.; He, X.; Yi, M.; Xi, C. Characterization of pore structure and the gas diffusion properties of tectonic and intact coal: Implications for lost gas calculation. *Process Saf. Environ. Prot.* **2020**, *135*, 12−21.
(42) Yin, S.; Song, D.; Li, J.; He, X.; Qiu, L.; Lou, Q.; Wei, M.; Liu, Y. Research on electromagnetic radiation (EMR) waveform characteristics of coal failure process using Hilbert-Huang transform (HHT). *Measurement* **2022**, *187*, No. 110195.
(43) Kumar, C. V.; Vardhan, H.; Murthy, C. S. N.; Karmakar, N. C. Estimating rock properties using sound signal dominant frequencies during diamond core drilling operations. *J. Rock Mech. Geotech. Eng.* **2019**, *11*, 850−859.

https://doi.org/10.1021/acsomega.3c01815
ACS Omega 2023, 8, 15799−15809